Vol. 508: 87–103, 2014
doi: 10.3354/meps10835

MARINE ECOLOGY PROGRESS SERIES
Mar Ecol Prog Ser

Published August 4

Zooplankton distribution and transport in the California Current off Oregon

D. Wu[1], M. Zhou[1,*], S. D. Pierce[2], J. A. Barth[2], T. Cowles[2]

[1]University of Massachusetts Boston, 100 Morrissey Blvd, Boston, MA 02125, USA
[2]Oregon State University, 104 Kerr Administration Building, Corvallis, OR 97331, USA

ABSTRACT: Transport and retention of zooplankton biomass in the shelf and slope regions off Oregon, USA, were studied in June 2002, using high-resolution measurements of temperature, salinity, depth, fluorescence, water current and zooplankton abundance. We employed 2 different analytical methods for minimizing divergence in the geostrophic current fields based on measurements from a vessel using an acoustic Doppler current profiler. We detected high zooplankton biomass in coastal upwelling areas on the shelf, and exchanges between shelf waters with high zooplankton biomass and offshelf waters with low zooplankton biomass via cross-isobath currents. In the shelf area of Heceta Bank off Newport bounded by the 153 m isobath, the standing zooplankton biomass was ~4 × 10^4 t C. The major flux of zooplankton biomass into the area occurred at the northern boundary at a rate of 1 × 10^3 to 2.5 × 10^3 t C d^{-1} or a specific rate of 0.03 to 0.06 d^{-1} based on 2 different analytical methods. The flux at the southern boundary was 1 order of magnitude lower, and a significant flux out of the area occurred at the 153 m isobath at a rate of ~0.8 × 10^3 to 3.7 × 10^3 t C d^{-1} or a specific rate of 0.02 to 0.09 d^{-1}. These rates are comparable with the zooplankton growth and mortality rates of ~0.1 d^{-1} previously reported for this region. Offshelf transport of zooplankton contributes significantly to biomass losses in shelf ecosystems and in turn fuels offshelf ecosystems.

KEY WORDS: Shelf · Coastal retention · Physical-biological coupling · Productivity

INTRODUCTION

The California Current system off the Oregon and California coasts is highly productive during spring and summer upwelling seasons. The association of these high productivities with mesoscale physical features has sparked a number of scientific studies on physical, chemical and biological processes and the sustainability of fisheries within the California Current. The Coastal Ocean Dynamics Experiment in the early 1980s revealed that the intensive offshore jets associated with cold filaments penetrated more than 100 m deep and transported coastal biota from the shelf to hundreds of kilometers off the shelf (Kosro & Huyer 1986). The data from the Ocean Prediction Through Observations, Modeling, and Analysis Experiment of 1982–1986 showed that surface jets and eddies were more energetic in the summer than in the winter (Rienecker & Mooers 1989, Strub et al. 1991). The Coastal Transition Zone Experiment in the late 1980s concluded that the cold filaments originated from continuous, meandering jets which separated onshelf and offshelf waters (Strub et al. 1991), and that deep phytoplankton layers in the offshelf water originated from the subducted coastal cold water at the transition or converging zone (Brink & Cowles 1991). In the early 1990s, the Northern California Coastal Circulation Study discovered that the velocity variability on time scales from weeks to months was produced by mesoscale eddies moving off the shelf (Largier et al. 1993). The Eastern Boundary Current Project was conducted in the early 1990s,

*Corresponding author: meng.zhou@umb.edu

focusing on mesoscale variability of physical and biological fields. Results from this project indicated that maxima of zooplankton abundance and biomass coincided with mesoscale eddies (Huntley et al. 1995). Processes of zooplankton transport and population dynamics associated with these mesoscale eddies were further studied using the size-structured zooplankton model and objective interpolation method, revealing that the generation time scale of mesozooplankton and macrozooplankton varies from 30 to 100 d (Huntley & Lopez 1992, Zhou & Huntley 1997, Zhou et al. 2001). Assuming a current of ~10 cm s^{-1}, the advective time scale over a mesoscale or topographic feature of 50 to 100 km is ~6 to 12 d, which is much smaller than the generation time scale (Huntley & Lopez 1992, Zhou et al. 2001). Thus, the effects of advection processes on zooplankton distribution and productivity are expected to be on the first order of magnitude compared to other physical, chemical and biological processes.

The California Current is generally southward, close and parallel to the coast north of Newport, Oregon (Barth et al. 2000, 2005). The bathymetry of the region leads to the formation of mesoscale eddies or meanders over Heceta Bank, which entrap upwelled cold water near the coast. Frequently, mesoscale eddies and filaments spin off from the coast and translate westward. The California Current separates from the coast at Cape Blanco and flows southwestward (Kosro et al. 1991, Barth et al. 2000). A subsurface northward undercurrent of 5 cm s^{-1} was observed between 35° and 50°N along the shelf break in the depth range between 125 and 325 m (Pierce et al. 2000). In the upper 200 m, the vertically integrated volume transports of the southward California Current and the northward undercurrent are ~3 and 0.8 Sverdrup, respectively (Barth et al. 2000, Pierce et al. 2000). The dynamics of these mesoscale features are associated with baroclinic instability of the California Current (Pierce et al. 1991), topographic features (Haidvogel et al. 1991), and wind stress (McCreary et al. 1991). Biological processes are coupled with mesoscale physical processes in the California Current (Huntley et al. 1995, Zhou & Huntley 1997, Barth et al. 2002). Phytoplankton and zooplankton biomasses enhanced by upwelling in coastal areas will be either transported away by the California Current or retained by eddies and meanders.

To understand the fate of zooplankton in eddies and jets requires resolving zooplankton distributions and processes at the scale of eddies and jets. Significant efforts have been made in the last 2 decades using towed optical and acoustic devices to resolve both physical and biological fields at the same location and time, e.g. in the California Current system (Huntley et al. 1995, Zhou et al. 2001, Barth et al. 2002), in the Georges Bank region (Wiebe et al. 2001, Benfield et al. 2003, Ullman et al. 2003) and in northern Norwegian shelf areas (Fossheim et al. 2005, Zhou et al. 2009, Zhu et al. 2009). Although results from these early studies elucidated qualitative relationships between physical and biological fields, quantitative estimates of transport and retention of zooplankton biomass and the rates of zooplankton population dynamic processes were rarely found. To elucidate these process rates, the physical processes of advection and retention need to be resolved.

A cruise was conducted between 1 and 17 June 2002 as part of the US Global Ocean Ecosystems Dynamics Program (GLOBEC) Northeast Pacific Study (NEP) for surveying physical and biological fields using towed and shipboard physical-biological sensors (Barth et al. 2005). Here, we use these integrated physical and biological data to make quantitative estimates of transport, retention and process rates, potential errors based on different analytical methods, and limits of survey and analytical methods. Our aim was to assess local food web dynamics.

MATERIALS AND METHODS

Data

The study area extended from 44° 37′ N off Newport, Oregon, to 41° 44′ N off Crescent City, California, and from the coast to ~100 km offshore (Fig. 1). The mesoscale survey was conducted over a period of 5 d with 7 cross-shelf transects ~0.25° latitude apart. Two fine-scale surveys were then conducted in the Heceta Bank and Cape Blanco regions, with 8 cross-shelf transects at latitudinal intervals of ~0.05° to 0.15° (Fig. 1). A towed SeaSoar instrument package was employed during the survey and included 2 pairs of SBE 911 plus conductivity, temperature and depth sensors (CTD; Sea-Bird Electronics) for the hydrographic data, a flourometer (Wet Lab) for relative fluorescence as a proxy of phytoplankton biomass, and an optical plankton counter (OPC; Focal Technologies) for zooplankton sized between 0.25 and 2.4 cm in equivalent spherical diameter (ESD). The SeaSoar undulated from the surface to ~10 m above the bottom in coastal areas, or a maximum depth of ~200 m in offshore areas at a ship speed of 7 to 8 knots. The SeaSoar undulating cycle varied from

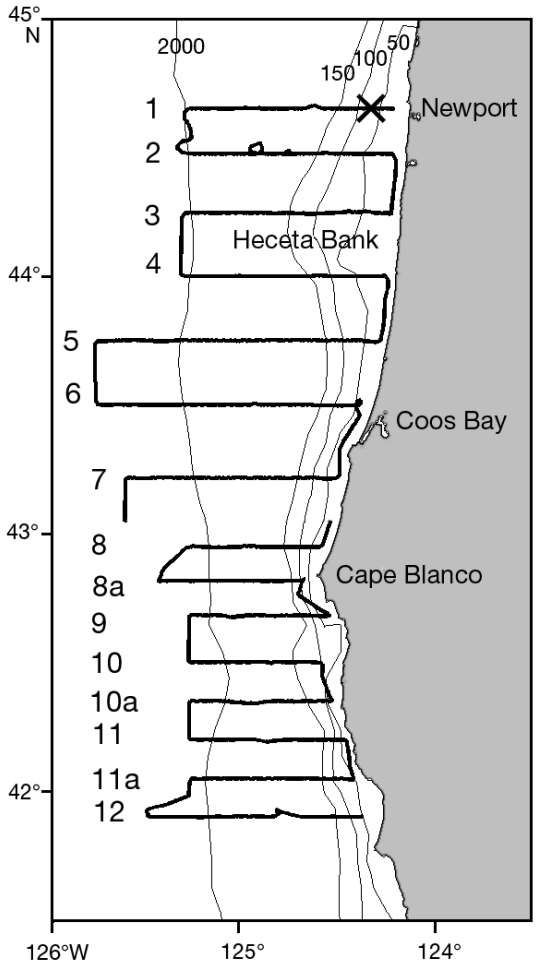

Fig. 1. Bathymetry of the study area off Oregon. The thin black lines are 50, 100, 150 and 2000 m isobaths, the thick black lines represent 15 transects including 7 mesoscale survey transects from 1 to 7 and 8 southern fine-scale survey transects from 8 to 12. Black cross at Transect 1: location of NOAA NDBC Station 46050

1.5 min on the shelf to 16 min off the shelf, which led to horizontal resolutions of 350 m and 4 km on and off the shelf, respectively. The highest vertical resolutions of physical and biological data were determined by the SeaSoar undulation speed and sampling rates of the CTD at 24 Hz, and both fluorometer and OPC at 2 Hz. Due to OPC failure, there were no OPC data collected for Transects 8 to 12 of the mesoscale survey. Thus, in this study the mesoscale transects 8 to 12 were replaced by the fine-scale survey off Cape Blanco.

A vessel-mounted 153 kHz narrow band (NB) acoustic Doppler current profiler (ADCP; RD Instruments) was used for current measurements with the bin length of 8 m and ensemble average of 5 min. The error in 5 min averaged velocities was 0.04 and 0.02 m s^{-1} using navigation and bottom track, respectively (Barth et al. 2005). Wind measurements were obtained from NOAA's National Data Buoy Center for Station 46050 located at 44° 37′ N, 124° 30′ W, ~37 km offshore of Newport, Oregon (www.ndbc.noaa.gov). Zooplankton taxonomic data were based on live samples collected on 31 May 2002 over Heceta Bank using a 0.5 m^2 ring net with 202 µm mesh towed in the upper 100 m at 1 knot (Fig. 1) (W. Peterson unpubl. data).

Data processing

The OPC provides plankton counts in 3494 digital sizes corresponding to a size range between 0.25 and 24 mm in ESD (Herman 1992). To use the carbon unit, the ESD of a zooplankter was converted to its body carbon based on the equation of Rodriguez & Mullin (1986) developed specifically for the California Current system by assuming the length to width aspect ratio of 1.61 for copepods (Huntley et al. 2000):

$$\log_{10}(\mu g\ C) = 2.23\log_{10}(ESD\ in\ \mu m) - 5.58 \quad (1)$$

To strengthen statistical means and standard deviations of measurements in a given size interval, 3494 body carbon sizes were integrated into 50 body carbon size intervals on an equal $\log_{10}$ basis. Within each size interval, cumulative biomass (µg C) of zooplankton was computed for every 0.5 s and then normalized by the water volume filtered (m^3) and size interval (µg C) that leads to a normalized biomass spectrum (per m^3) following Platt & Denman (1978) and Zhou & Huntley (1997) (referred to hereafter as biomass spectrum). All OPC data were processed along the undulating paths for the mesoscale and fine-scale surveys. It should be kept in mind that the uncertainty of OPC measurements in zooplankton biomass estimates is significant due to different optical properties of zooplankton species and spatial variation of taxonomic compositions (Herman 1992). This uncertainty can have an effect on evaluating the bias of physical processes on process rate estimates (Huntley et al. 1995).

To compute coupled physical and biological data and variables, all CTD, fluorometer and OPC data were further processed into 8 m vertical bins to match the ADCP data. Because the first depth bin of ADCP measurements started at 25 m, all CTD, fluorometer and OPC data in the upper 25 m were averaged. At each depth bin, all data were interpolated into 50 × 50 horizontal grids using the objective interpolation method within the survey area boun-

ded by 41° 54′–44° 40′ N and 124° 08′–125° 46′ W (Fig. 1) (Bretherton et al. 1976, Zhou 1998, Barth et al. 2000).

The spatial decorrelation scales and covariance functions were determined from the autocorrelations of temperature data from CTD in the zonal and meridional directions based on Legendre & Legendre (1983). The zonal correlations were computed at individual longitudinal transects, and then the mean zonal correlation was obtained by taking a latitudinal average. For the mean meridional correlation, we first binned the data into 0.15° longitudinal bins along each transect, computed the meridional correlation at a given longitude and then averaged meridional correlations longitudinally. The minimum latitudinal scale of physical and biological features was determined by the distance between 2 transects, i.e. ~0.25°. The results indicated an anisotropic field with the decorrelation scales of 33 and 88 km in the zonal and meridional directions, respectively (see Fig. 3), both of which are much larger than the spatial resolutions in the datasets. The decorrelation scales were consistent with that estimated from the time series of current data off Oregon (Kundu & Allen 1976). An appropriate covariance function $(1-r)e^{-r}$ was selected to fit autocorrelation data where $r = \sqrt{(\Delta x/l_x)^2 + (\Delta y/l_y)^2}$, l_x and l_y are the decorrelation scales in the zonal and meridional directions, and Δx and Δy are the distances between 2 locations in longitude and latitude.

To remove barotropic tidal current components from ADCP current measurements is challenging, because errors can be introduced by measurements, tidal currents predicted from a tidal model and the interpolation method used for gridding. The tidal currents predicted from a tidal model were extracted based on the location and time along the ship track (Erofeeva et al. 2003), and the detided currents were obtained by subtracting the predicted tidal currents from the ADCP current measurements. Because there is no streamfunction for tidal currents, fitting a streamfunction to detided currents during interpolation will further remove tidal and ageostrophic components. We used 2 objective interpolation methods developed by Barnes (1964) and Bretherton et al. (1976) (referred to hereafter as Barnes and BDF interpolations, respectively). Barnes interpolation is a successive correction method, which minimizes differences between passes under defined decorrelation scales. The streamfunction is calculated based on Hawkins & Rosenthal (1965). BDF interpolation is based on statistics and defined decorrelation scales, and the streamfunction is obtained by minimizing divergences (Bretherton et al. 1976, Dorland & Zhou 2008). Although these 2 mathematical interpolations are both valid and well tested, the differences in results between these 2 different methods will bring insight into the sensitivities and uncertainties involved in interpreting population dynamic processes.

We tested 2 spatial covariance functions for Barnes interpolation, of which one is an isotropic covariance function with decorrelation scales of 50 km in both zonal and meridional directions to match previous studies (Huntley et al. 1995), and the other is an anisotropic covariance function with decorrelation scales of 33 km in the zonal direction and 88 km in the meridional direction, which match the decorrelation scales computed from our data. Two passes were applied for both covariance functions, and the velocity differences between 2 passes were <1 cm s^{-1}. We found no differences in means and spatial patterns between these 2 different covariance functions. For consistency with previous studies, the results from the isotropic 50 km Barnes interpolation are presented in this paper. Because BDF interpolation will maximize mesoscale features at the defined spatial scales, we used the anisotropic covariance function with scales of 33 km in the zonal direction and 88 km in the meridional direction. The numerical divergences of interpolated current fields were in the order of 10^{-7} and 10^{-18} s^{-1} for Barnes and BDF interpolations, respectively.

Transport theories

For zooplankton biomass (b), the local change is primarily determined by the convergence of biomass transport, and the bio-reaction related to the population dynamics processes:

$$\frac{\partial b}{\partial t} = R(b,t) - \left(\frac{\partial ub}{\partial x} + \frac{\partial vb}{\partial y} + \frac{\partial wb}{\partial z} \right) \quad (2)$$

where t is time, and u, v and w are the zonal (x), meridional (y) and vertical (z) velocity components, respectively. On the right side of Eq. (2), $R(b,t)$ represents the bio-reaction (a net production), and the second term presents the advection or convergence of zooplankton transports. In order to examine the total biomass variation, we integrate Eq. (2) over the depth of the water column (H), assuming there is no flux crossing the surface and bottom:

$$\frac{\partial}{\partial t}\int_H^0 b\,dz = \int_H^0 R(b,t)\,dz - \left(\frac{\partial}{\partial x}\int_H^0 ub\,dz + \frac{\partial}{\partial y}\int_H^0 vb\,dz \right) \quad (3)$$

In Eq. (3), the term on the left side is the local change rate of vertically integrated biomass in the water column. On the right side, the first and second terms are the bio-reaction and convergence of horizontal transport, respectively. The horizontal transport can be calculated directly from binned current and OPC data. The horizontal convergence of biomass can be further separated into 2 terms as:

$$-\left(\frac{\partial}{\partial x}\int_H^0 ub\,\mathrm{d}z+\frac{\partial}{\partial y}\int_H^0 vb\,\mathrm{d}z\right)= -\int_H^0\left(u\frac{\partial b}{\partial x}+v\frac{\partial b}{\partial y}\right)\mathrm{d}z-\int_H^0 b\left(\frac{\partial u}{\partial x}+\frac{\partial v}{\partial y}\right)\mathrm{d}z \quad (4)$$

On the right side, the first term is the biomass convergence contributed by gradient advection, and the second term is the retention of b determined by current convergence. This current convergence term should be small, because the flow field at the spatial scale of our interest is nearly geostrophically balanced (Kosro & Huyer 1986, Shearman et al. 2000, Pickett & Paduan 2003). The current convergence estimates are on the second order resulting from either the Ekman pumping driven by wind stress curl or the secondary circulation determined by the quasi-geostrophic dynamics. Thus, in a heterogenic zooplankton field, the advection of zooplankton gradients should play the dominant role in concentrating or dissipating zooplankton.

The sign of the biomass gradient advection implies a high biomass or a low biomass center moving into an area. When a positive (negative) current advects a negative (positive) gradient, the higher biomass is moving in what we refer to as a positive gradient advection. When a positive (negative) current advects a positive (negative) gradient, the lower biomass is moving in what we refer to as a negative gradient advection.

To examine the productivity of a given region, a Eulerian control water volume (V) can be selected. For example, a control water volume for the Oregon coastal region can be bounded by Transects 1 and 12 latitudinally, by the coast and the 153 m isobath longitudinally, and by the surface and bottom vertically. Integrating Eq. (3) over an area (S) bounded by the boundary (δS) and water depth (H), and applying Stokes' theory (Beyer 1987) results in:

$$\frac{\partial}{\partial t}\int_S\int_H (b\,\mathrm{d}z)\mathrm{d}S= \int_S\int_H [R(b,t)\mathrm{d}z]\mathrm{d}S-\oint_{\delta S}\left[\left(\int_H^0 ub\,\mathrm{d}z\right)\mathrm{d}y+\left(\int_H^0 vb\,\mathrm{d}z\right)\mathrm{d}x\right] \quad (5)$$

Eq. (5) again represents the balance between biomass change in a control region, local net production and transport fluxes.

The errors in the estimation of biomass transports stem from errors in both current and zooplankton biomass estimates. Theoretically, the errors of the estimated streamfunctions and zooplankton distributions should be known, because the interpolations are based on statistics and given covariance functions (Bretherton et al. 1976, Barth et al. 2000). However, the detided ADCP current measurements include unknown errors in ship movements, modeled tidal currents and ageostrophic currents. Zooplankton measurements include unknown errors due to zooplankton patchiness, and migration and avoidance behavior. We cannot quantify these errors and do not know their statistical characteristics.

Zooplankton diel vertical migration

To evaluate the effects of zooplankton vertical migration on zooplankton biomass estimates, the OPC data were separated into day- and nighttime based on PAR (photosynthetically available radiation), which was predicted as a function of latitude and day of the year. The night period was defined as PAR = 0, corresponding to approximately 19:00 to 05:00 h local time during the survey period. Daytime and nighttime biomass spectra were constructed between the surface and the maximum depth the SeaSoar reached. We exclude the coastal area shallower than 153 m isobath for this study because high biomass measurements in shallow coastal regions could lead to high biomass estimates in upper water columns and bias the estimates.

To compare biomass distributions between daytime and nighttime, the depth center (z) of biomass distribution was determined as:

$$z=\sum_i B_i\cdot z_i \Big/ \sum_i B_i \quad (6)$$

where B_i is the biomass at the depth of z_i, and i is the index of depth layers. A 2-sample t-test was used to test for significant differences ($p < 0.05$) in vertical biomass distributions between daytime and nighttime. To compute the depth center of biomass distribution in the water column, the zooplankton biomass data were binned into 8 m depth bins from the surface to 153 m, and then averaged along the ship track using a longitudinal interval of 0.05°.

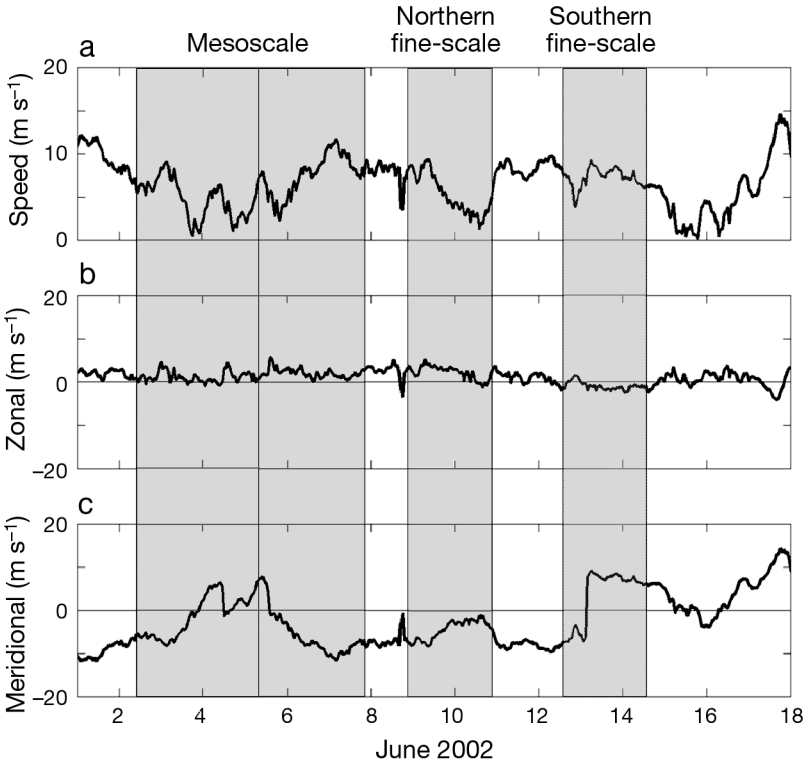

Fig. 2. The time series of wind measurements at NOAA NDBC Station 46050 during the survey period: (a) wind speed, (b) zonal component and (c) meridional component. The shaded areas indicate the periods of the mesoscale, northern and southern fine-scale surveys

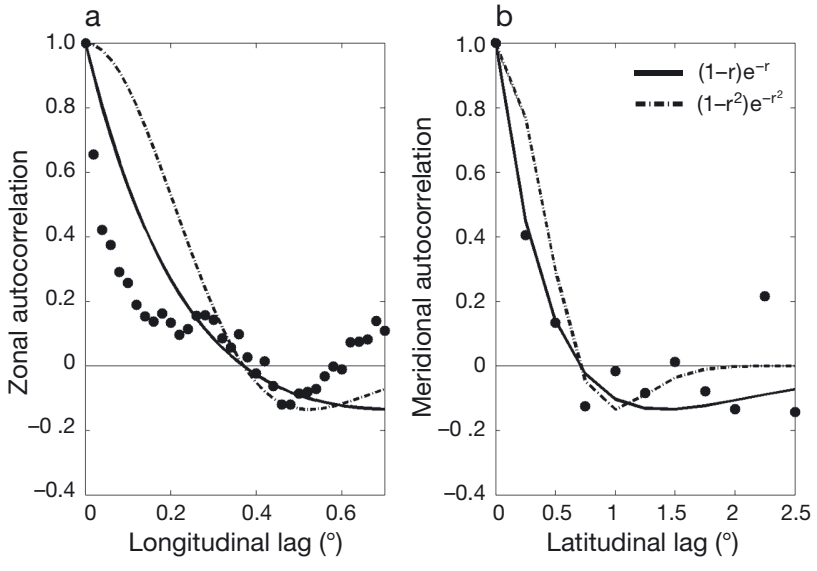

Fig. 3. Autocorrelations calculated from temperature data: (a) zonal and (b) meridional components. The black dots are calculated data, the dashed lines are the best-fit covariance function $(1-r)e^{-r}$, and the solid lines are the best-fit covariance function $(1-r^2)e^{-r^2}$. The zero crossings are 33 and 88 km in the zonal and meridional directions, respectively

RESULTS

Wind condition

The wind during the survey period (2–15 June 2002) was predominately southward and upwelling-favorable, with a maximum wind speed of ~10 m s^{-1} (Fig. 2). There were 2 northward wind events on 4 and 13 June 2002. The first event lasted ~2 d and occurred in the second half of the mesoscale survey, while the second event lasted <2 d and occurred in the southern fine-scale survey. The predominately upwelling-favorable wind, short-term relaxation and downwelling-favorable wind led to upwelling and downwelling.

Horizontal patterns of temperature, currents, chlorophyll and zooplankton

The results from the autocorrelation analysis of CTD data indicate an anisotropic field (Fig. 3). In the zonal direction, the autocorrelation decreases quickly within 18 km, becomes flat between 18 and 27 km, and has the first zero-crossing at 33 km, which implies the existence of multiple scales. In the meridional direction, the autocorrelation decreases monotonically, crossing the zero at 88 km. The fits using different theoretical functions were tested. The covariance function of $(1-r)e^{-r}$ was the best fit and chosen for the interpolations of temperature, chlorophyll, zooplankton abundance and biomass, and currents (see Figs. 4 to 9).

The coastal upwelling area can be identified from the colder water at the surface along the Oregon and northern California coasts compared to the warmer water in the offshore areas (Fig. 4a). Between Newport and Cape Blanco, Oregon, the upwelling area was parallel to the coast within a narrow 10 to 20 km band, while south of Cape Blanco, the upwelling area ex-

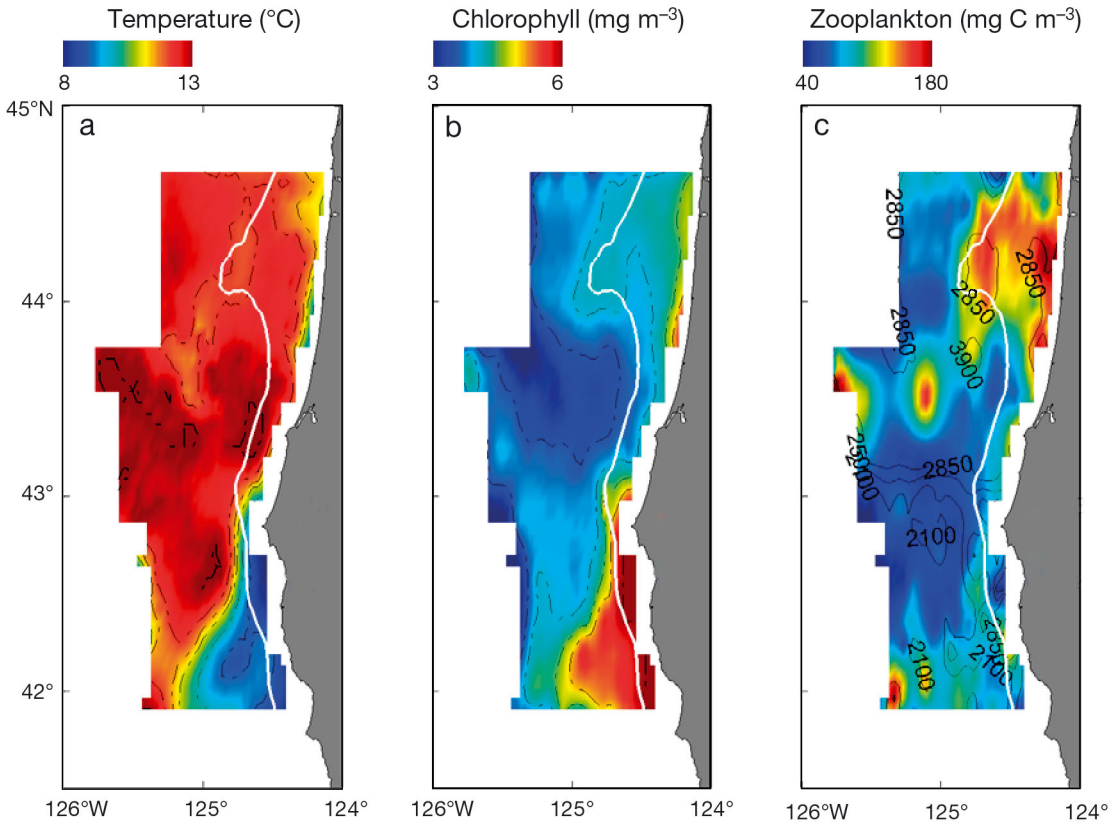

Fig. 4. Horizontal patterns at 5 m depth: (a) temperature, with black dash contours at 1°C intervals; (b) chlorophyll distribution, with black dash contours at 1 mg m^{-3} intervals; and (c) zooplankton biomass distribution, with solid black contours representing zooplankton abundance (ind. m^{-3}). Solid white contour line: 153 m isobath

tended ~100 km offshore. Associated with these upwelling fronts, the currents from streamfunctions best-fitted with the detided currents from the mesoscale survey revealed jets and eddies (Fig. 5). On Heceta Bank, the cold water of 10°C started inshore and spread over the bank area (Fig. 4a). South of Cape Blanco, associated with the broad upwelling area, the California Current departed from the coast in a southwestward direction (Fig. 5a). From Barnes interpolation, the California Current was steered offshore at Heceta Bank and Cape Blanco forming meanders (Fig. 5b), while from BDF interpolation, eddies were clearly formed over Heceta Bank and off Cape Blanco (Fig. 5c). The spatial patterns from these 2 interpolations are very different due to different inherent assumptions in the methods. Though both results are valid because both interpolation methods are well developed and tested, the significant differences in results have demonstrated the challenges in resolving physical processes and transport-retention of zooplankton populations.

Because the OPC failed in the second half of the mesoscale survey, we used the CTD, fluorometer and OPC data from the mesoscale survey Transects 1 to 7 and the southern fine-scale survey transects (see Fig. 1). The chlorophyll distribution at 5 m was highly correlated with the upwelled cold water, while the zooplankton biomass distribution at 5 m was not correlated with the upwelled cold water (Fig. 4b,c). Elevated chlorophyll and zooplankton concentrations were found in the mesoscale eddy and the offshore transported cold water near Heceta Bank and in the broad upwelling area south of Cape Blanco. Offshore transports of phytoplankton and zooplankton by the California Current were found in Areas 2 and 3 west of Heceta Bank, while offshore water with low chlorophyll and zooplankton concentrations intruded into the coastal area between Heceta Bank and Cape Blanco through the low temperature tongue in Area 4 (see Fig. 6a).

The spatial patterns in the mean zooplankton abundance and biomass distributions between the surface and 153 m depth can be visually linked to the temperature patterns and mesoscale features of jets and eddies (Fig. 6). High zooplankton abundances and biomass were found along all coastal upwelling

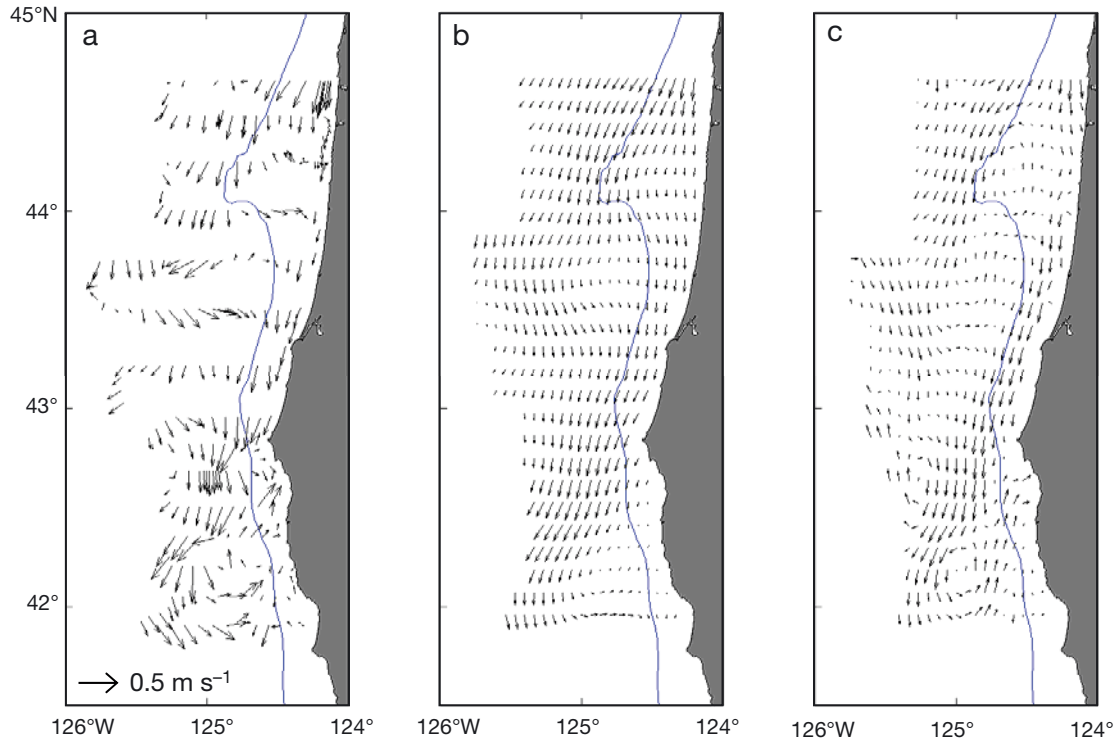

Fig. 5. Horizontal current (m s^{-1}) patterns at 25 m depth, represented by vectors: (a) 30 min averaged detided acoustic Doppler current profiler (ADCP) currents, (b) currents derived from Barnes interpolation, and (c) currents derived from the BDF interpolation. Solid blue line: 153 m isobath

areas, implying the effects of upwelling on primary and secondary productions. Zooplankton abundance maxima were found in most coastal areas, while zooplankton biomass maxima were found only over the Heceta Bank and Coos Bay areas (Fig. 6).

Vertical patterns of temperature, currents, chlorophyll and zooplankton

The coastal upwelling and offshore stratification are indicated by the outcropped thermocline along mesoscale Transect 5 (Fig. 7a). The upwelling area was limited near the coast, with temperatures as low as 7 to 8°C. Crossing the upwelling front, the water was stratified, with surface temperatures of 12 to 14°C and a thermocline depth of 20 to 30 m. Based on ADCP current measurements, jets and eddies were associated with the slopes of the thermocline (Fig. 7a).

Between 125° 00′ and 125° 15′W on Transect 5, a southwestward jet at ~30 cm s^{-1} was found (Fig. 5b), consistent with the offshore-ward California Current at Heceta Bank (Barth et al. 2005). The along-transect current component showed a convergent pattern in the upper 150 m within this jet in those areas where the water depth is >180 m (Fig. 7a). This zonal convergence may lead to the deep penetration of phytoplankton and zooplankton biomasses (Fig. 7b,c).

The surface chlorophyll maximum was found in the nearshore upwelling area (Fig. 7b), and the subsurface maxima were found near the thermocline in the offshore stratified water column. Corresponding to such phytoplankton distributions, zooplankton were distributed over the entire water column (with surface enhancements in the nearshore area) and strongly correlated with phytoplankton maxima in offshore areas (Fig. 7c).

Zooplankton biomass transport

The horizontal transport vectors of zooplankton biomass within the upper 153 m were calculated based on OPC biomass measurements and 2 current fields from Barnes and BDF interpolations (Fig. 8). All of them show similar large-scale patterns, for example the dominant offshore and southward transports of zooplankton. The onshore and northward transports of zooplankton were only revealed when using BDF interpolation (Fig. 8c).

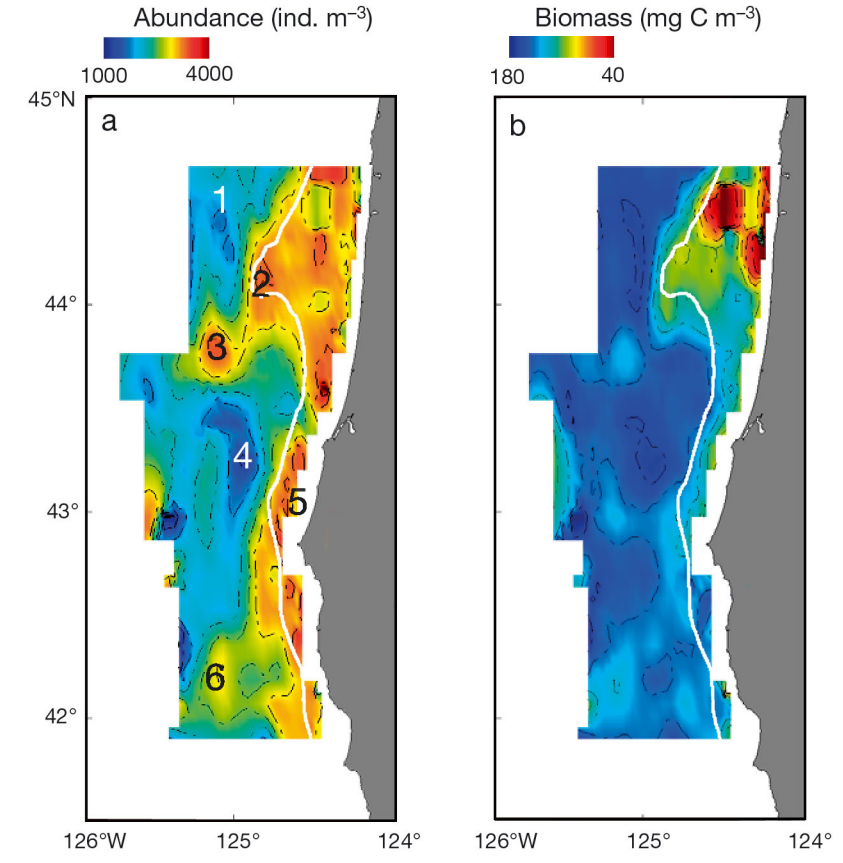

Fig. 6. Depth-averaged distributions between 0 and 153 m depth: (a) zooplankton abundance and (b) zooplankton biomass. Six 20 × 20 km areas are indicated in (a): (1) the southward jet area at the northern boundary, (2) the high-biomass area on Heceta Bank, (3) the high-biomass area within the southwestward jet off Heceta Bank, (4) the low-biomass area within the onshore return flow, (5) the high-biomass area in the coastal region north of Cape Blanco, and (6) the high-biomass area within the offshore jet southwest of Cape Blanco. Solid white line: 153 m isobath; dashed line: contour lines to separate different colors for enhancing patchy features

The depth-integrated zooplankton biomass gradient advection was calculated based on Eq. (4), using the OPC biomass measurements and the mesoscale current field based on BDF interpolation (Fig. 9a). Positive advection implies that water with higher zooplankton biomass is displacing water with lower biomass and vice versa. Negative advection was found in the onshore current south of Heceta Bank, where the shoreward current transported low biomass water northeastward. Positive values were found in coastal regions where the currents had transported higher zooplankton biomass into the area. Within the advection terms as expressed in Eq. (4), the advection of biomass gradients dominated the processes, especially in the areas of offshore transport. To compare the biomass advection with zooplankton growth rates, the specific convergence rate of biomass advection was computed using the ratio of depth-integrated biomass gradient advection to depth-integrated zooplankton

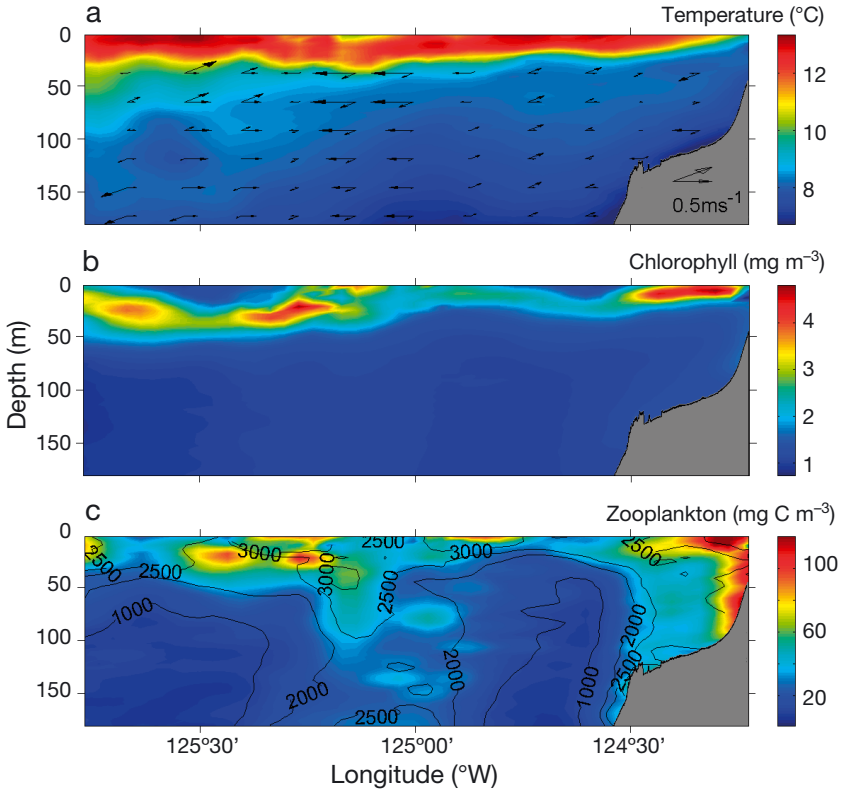

Fig. 7. Cross-shelf vertical patterns along mesoscale Transect 5: (a) temperature, with ADCP currents represented by the horizontal vectors for the zonal components and the 45° vectors for the meridional components; (b) chlorophyll; and (c) zooplankton biomass, with solid black contours representing zooplankton abundance (ind. m^{-3})

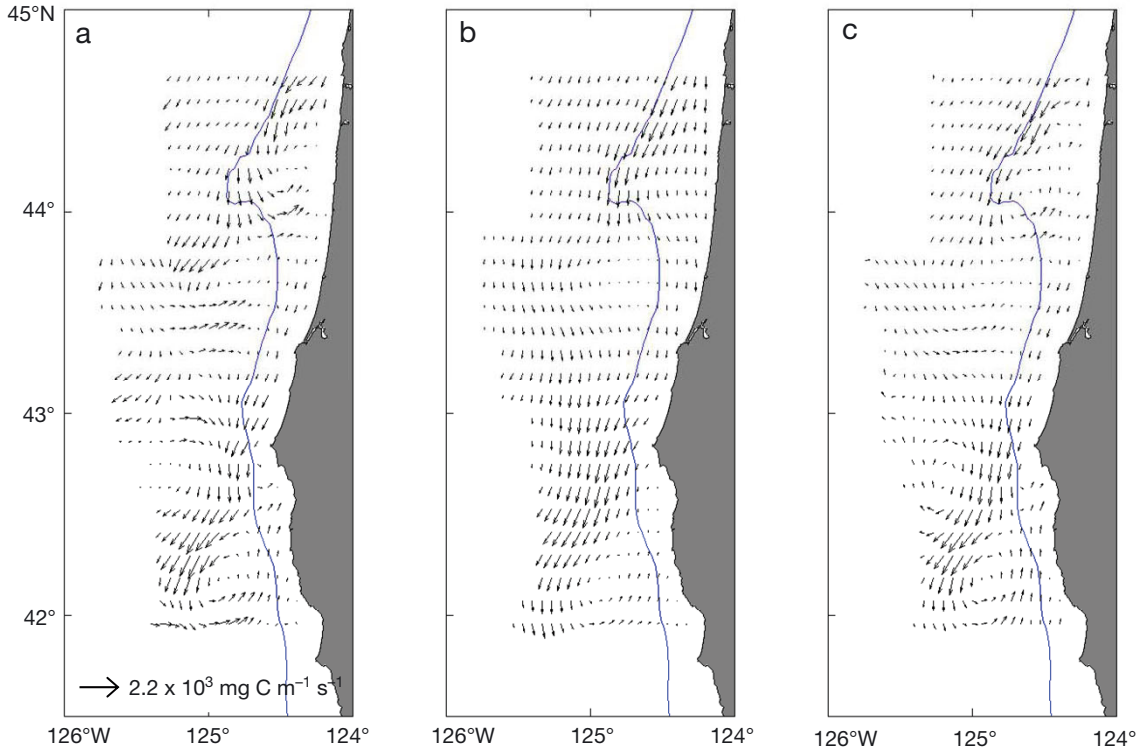

Fig. 8. Depth-integrated (0–153 m) horizontal transport of zooplankton biomass (mg C m^{-1} s^{-1}) derived from (a) 30 min averaged detided ADCP currents, (b) Barnes interpolation, and (c) BDF interpolation. Solid blue line: 153 m isobath

biomass in the survey area (Fig. 9b). The convergence rate varied between −0.5 and 0.5 d^{-1} in early June.

To estimate the magnitude of zooplankton biomass offshore transport and coastal retention, we defined a coastal area as bounded by the coast, the 153 m isobath, and Transects 1 and 12 (Fig. 1). Employing Eq. (5), the flux crossing the coast is equal to zero, and the transport fluxes crossing Transects 1 and 12 and the 153 m isobath were estimated based on the current fields from both Barnes and BDF interpolations (Table 1). The results show that the flux estimates are extremely sensitive to the current fields, especially the estimates at the 153 m isobath.

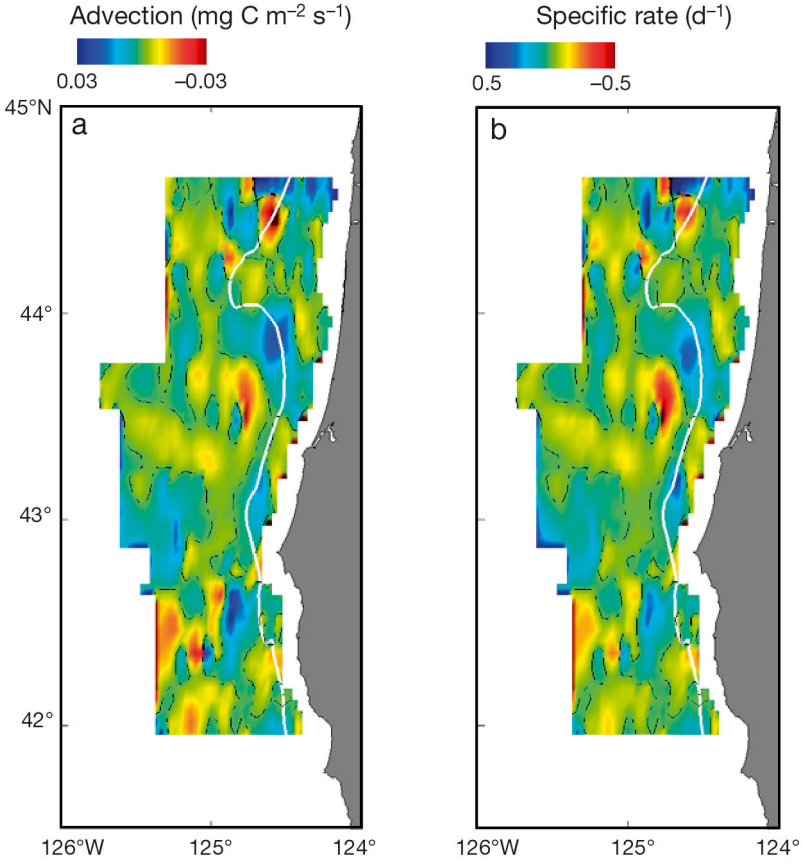

Fig. 9. Depth-integrated (0–153 m) (a) biomass gradient advection (mg C m^{-2} s^{-1}) derived from the BDF interpolation and (b) specific rate of biomass gradient advection (d^{-1}) based on the ratio of the depth-integrated biomass gradient advection to the depth-integrated biomass. Dashed lines: zero contours

Table 1. Zooplankton biomass transport fluxes ($\times 10^3$ t C d^{-1}) into the coastal area shallower than 153 m between 44° 37′ N (Transect 1) and 41° 44′ N (Transect 12) (Fig. 1), and corresponding rates (d^{-1}). A positive or negative value represents a net flux of biomass into or out of the coastal area, respectively. The rate estimate is based on the estimated total standing biomass of 4×10^4 t C within the control area. Data were calculated using 3 methods: detided acoustic Doppler current profiler (ADCP) currents and 2 different interpolation methods based on Barnes (1964) and BDF (Bretherton et al. 1976, Dorland & Zhou 2008) (see 'Materials and methods: Data processing')

Current field	— Transect 1—		—Transect 12 —		——153 m ——		—— Net ——	
	Flux	Rate	Flux	Rate	Flux	Rate	Flux	Rate
Detided ADCP currents	2.1	0.05	0.1	0.003	1.4	0.04	3.6	0.09
Streamfunction 1[a]	2.5	0.06	−0.2	−0.005	−3.7	−0.09	−1.4	−0.04
Streamfunction 2[b]	1.0	0.03	0.1	0.003	−0.8	−0.02	0.3	0.01

[a]Derived from an isotropic covariance function with a scale of 50 km
[b]Derived from an anisotropic covariance function with a zonal scale of 33 km and a meridional scale of 88 km

Zooplankton size structure and diel vertical migration

To investigate zooplankton size structures and species, 6 representative areas were selected in the survey area (Fig. 6a): (1) the offshelf low biomass area west of Heceta Bank, (2) the highly productive Heceta Bank region, (3) in the offshoreward jet off Heceta Bank with both chlorophyll and zooplankton maxima, (4) in the offshelf water with both low chlorophyll and zooplankton, (5) the nearshore chlorophyll and zooplankton biomass maxima off Cape Blanco, and (6) within the offshore jet with both chlorophyll and zooplankton maxima southwest of Cape Blanco. The biomass spectra in Fig. 10a–c are paired between offshelf Areas 1 and 4, between nearshore Areas 2 and 5, and offshore jet Areas 3 and 6. The regression relationship between daytime and nighttime biomass spectra (Fig. 10d) indicates the significant similarity ($y = 1.06x - 0.29$, $r^2 = 0.99$). Within this size range, the net tow samples in the same area (44° 15′ N, 124° 31′ W) and at the same time indicate that *Pseudocalanus* spp. and *Calanus marshallae*, 2 of the most common copepod species in Oregon upwelling areas (Peterson et al. 2002), represented 35 and 33% of the biomass composition, respectively, during our study period (Fig. 11).

The mesozooplankton biomass depth centers between daytime and nighttime were analyzed using the hourly averaged data for examining detailed diel vertical migration patterns (Fig. 12). The biomass depth centers varied between daytime (54 ± 21 m) and nighttime (60 ± 21 m) but the difference was not statistically significant (*t*-test, df = 174, p = 0.29).

DISCUSSION

Mesoscale current fields from two interpolation methods

Both Barnes and BDF interpolation methods and stream functions revealed coastal jets, meanders and eddies (Fig. 5b,c). The coastal jets and eddies are significantly steered by shallow banks and capes in the Oregon and northern California region (Brink & Cowles 1991, Barth et al. 2000, 2002). The 2 interpolations did not show the same patterns. For example, Barnes interpolation showed the California Current turning to an offshore direction and forming large cross-isobath currents and a meander over Heceta Bank, while BDF interpolation showed the formation of small cross-isobath currents and an eddy over Heceta Bank. Comparing both interpolation results to the original detided ADCP currents, Barnes interpolation provides a smoother large-scale circulation pattern with fewer mesoscale features, while BDF interpolation retains more detailed mesoscale features under the nondivergent condition. The differences in the circulation patterns between different interpolation methods result from the inherent assumptions within the methods.

The differences between current fields are critically important in understanding transport and retention mechanisms of biota in coastal areas such as Heceta Bank. Barnes interpolation showed a cross-isobath offshelf transport in the southwestern part of the bank, while BDF interpolation showed a much reduced cross-isobath current controlled by isobaths. The magnitude of cross-isobath currents plays an important role for the population dynamics of zooplankton on Heceta Bank. Because both these

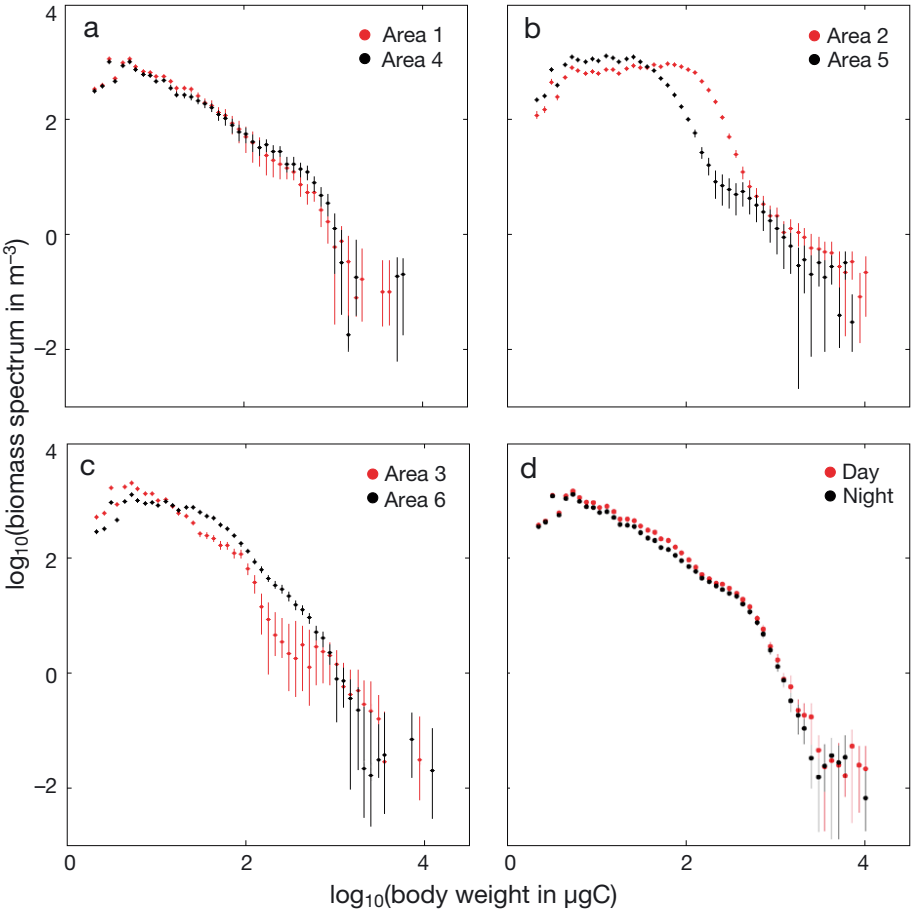

Fig. 10. Biomass spectra (mean ± 95% CI) from optical plankton counter (OPC) measurements in (a) Areas 1 and 4, (b) Areas 2 and 5, (c) Areas 3 and 6, and (d) during daytime (05:00–19:00 h) and nighttime (19:00–05:00 h) in the survey area deeper than 153 m. Areas are indicated in Fig. 6a

current fields are valid even though they focus on different features, caution is needed when choosing interpolation methods and current fields for computing transport and retention of biological fields. These methods were originally developed for analyzing and filtering imperfect *in situ* data for different objectives. Thus, advances in observation methods need to be made to obtain better measurements, and the analytical methods need to be chosen based on predominant physical processes.

Zooplankton maxima and mesoscale current fields

The meander or eddy over Heceta Bank can remain for several weeks according to Lagrangian drifter studies (Barth et al. 2000, van Geen et al. 2000). At Cape Blanco, the California Current separates from the coast and typically forms jets, meanders and eddies (Barth et al. 2000, 2005). These eddies and meanders increase the residence time of water masses and in turn can potentially affect phytoplankton and zooplankton productivity. The strong rela-

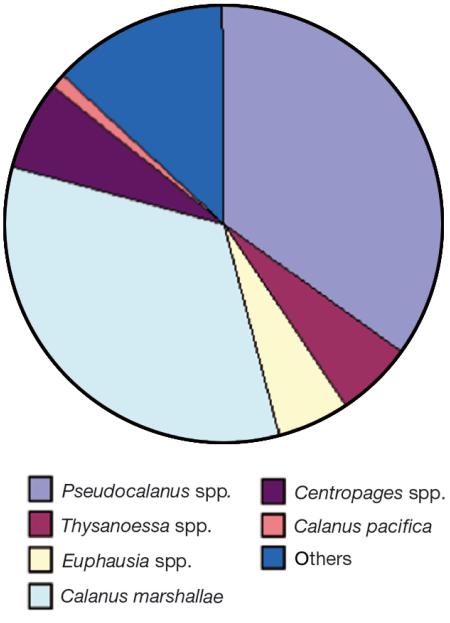

Fig. 11. Percentage composition of zooplankton species from zooplankton samples in the size range 16 to 250 µg C, collected in Area 2 off the Oregon coast (see Fig. 6a) in May 2002 (W. Peterson unpubl. data)

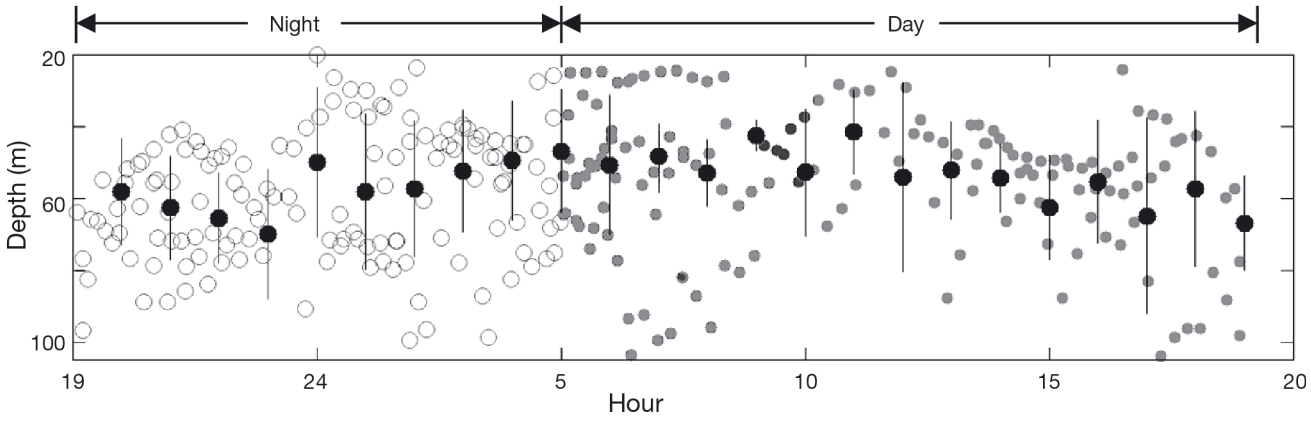

Fig. 12. Depth centers of zooplankton biomass derived from individual vertical profiles in the survey area deeper than 153 m as a function of (○) nighttime (19:00–05:00 h) and (●) daytime (05:00–19:00). (●): hourly means ± SD

tionships between coastal upwelling, eddies, chlorophyll concentrations and zooplankton biomass are clearly shown in Figs. 4 to 6, suggesting that upwelling drives the productive coastal ecosystem off Oregon and northern California.

In the Heceta Bank area, northward downwelling wind events did occur during the survey. Would a downwelling event erase chlorophyll and zooplankton maxima in nearshore areas? In a short downwelling wind event, the downwelling wind could prevent biota from being transported offshore and retain biomass along coastal regions by its onshore Ekman transport, so, chlorophyll and zooplankton maxima would remain. Thus, although currents varied between upwelling- and downwelling-favorable winds, the effect of enhanced productivity in coastal areas was persistent.

In offshelf areas, the zooplankton biomass maxima were associated with offshore-ward jets and meanders (Figs. 5 & 6). Some of these maxima could be related to the offshore transport by jets. For example, the deep zooplankton maximum between 125° 15′ and 124° 55′ W along Transect 5 (Fig. 7) was associated with an offshore-ward jet off Heceta Bank. Such offshore transports of phytoplankton and zooplankton biomasses have been observed in previous studies (Washburn et al. 1991, Huntley et al. 1995, 2000, Barth et al. 2002). Our study further shows the relationship between coastal productive areas and offshore zooplankton maxima associated with offshore-ward jets.

Zooplankton deep maximum

A zooplankton deep maximum was found along Transect 5 between 125° 15′ and 124° 55′ W longitude within the offshore jet region (Fig. 7). Similar chlorophyll and zooplankton deep maxima within the California Current system were also found in other studies (Huntley et al. 2000, Barth et al. 2002). The primary cause of deep biomass maxima may be the subduction of coastal biota with downwelling waters during offshore transport. In these deep maxima, both coastal and offshore zooplankton species can be found, representing the transport and mixing of coastal and offshore waters (Huntley et al. 1995).

The zooplankton deep maximum had a zonal scale of 40 km, which is equivalent to the internal Rossby radius in this area (Huyer 1983). No zooplankton deep maximum was found in either survey Transect 4 or 6, implying that the meridional scale of this deep maximum is less than 40 km. When jets and eddies are formed at the scale similar to the internal Rossby radius, their advection of zooplankton gradients could lead to the increase in zooplankton patchiness at similar scales.

In previous studies, the high abundances of phytoplankton biomass in deep waters were found to be associated with subduction of surface waters (e.g. Barth et al. 2002). The subduction mechanism is associated with the quasigeostrophic dynamics of jets and fronts that denser water tends to slide underneath less dense water (Rudnick 1996, Shearman et al. 2000, Barth et al. 2002). In the offshore-ward currents off Heceta Bank and Cape Blanco, the upwelled deep water near coasts could subduct near upwelling fronts with coastal biota and then be transported offshore with the currents that led to a convergent zone or subduction zone of zooplankton around the currents.

We found no significant difference between daytime and nighttime zooplankton biomass spectra (Fig. 10d). This result is different from findings in

high latitudes where krill migrated to the surface layer at the beginning of sunset and then spread into a broad water column depending on prey fields (Zhou et al. 2005), and in low latitudes where the migration patterns of mesopelagic boundary communities could be complicated by different migration speeds of different species (Benoit-Bird & Aub 2003). The similarity between daytime and nighttime zooplankton biomass spectra is consistent with the mesozooplankton biomass depth center analysis. Zooplankton did not aggregate in the upper water column more during the night than during the day. Previous studies also found that total copepod biomass and individual species showed no day–night difference in either net or OPC samples in the California Current region (Mackas et al. 1991, Huntley et al. 1995, Peterson et al. 2002).

Effects of advection on zooplankton community structure

The biomass spectra from 6 selected areas (Fig. 6a) all showed high abundance of zooplankton in small size classes and low abundance of zooplankton in large size classes (Fig. 10). This pattern has been observed in most ocean and freshwater environments (Sheldon & Parsons 1967, Sheldon et al. 1972, Rodriguez & Mullin 1986, Sprules & Munawar 1986). Results from net samples collected over Heceta Bank during the same period as our surveys indicate that the zooplankton assemblage in the body size range between 10^0 and 10^3 µg C in the California Current was dominated by a small number of species (W. Peterson unpubl. data), similar to previous findings (Huntley et al. 2000). Samples of body sizes between 0.5 and 1100 µg C contained early to adult stages of copepod species (*Pseudocalanus* spp., *Acartia* spp., *Centropages* spp., *Calanus marshallae* and *Calanus pacificus*) and early stages of *Euphausia pacifica* and *Sergestes similis*. Samples of body sizes larger than 1100 µg C were dominated by middle to adult stages of *E. pacifica*, *S. similis* and *Thysanoessa spinifera* (W. Peterson unpubl. data). These results are similar to previous findings (Mackas et al. 1991, Huntley et al. 2000, Peterson et al. 2002).

Biomass spectrum values for the size range between 16 and 250 µg C (1.2 to 2.4 on the $\log_{10}$ scale) over Heceta Bank (Area 2) were higher than those of other areas (Fig. 10). Within this size range, the net tow samples in approximately the same area (44° 15′ N, 124° 31′ W) and at the same time indicate that *Pseudocalanus* spp. and *Calanus marshallae*, 2 of the most common copepod species in Oregon upwelling areas (Peterson et al. 2002), represented 35 and 33% of biomass composition, respectively, during our study period (Fig. 11). Such elevated biomass spectra compared to the linear relationship have also been found in other coastal regions during spring, e.g. on the Norwegian shelf, where the elevated biomass spectra were the result of high abundances of *Calanus finmarchicus* copepod stage V and adults, and euphausiid larvae (Zhou et al. 2009).

Two types of biomass spectra were observed during our survey: the linear spectra found in the offshore area (Area 1) and along the onshore intruding current (Area 4); and the nonlinear spectra found in coastal upwelling areas (Areas 2 and 5) and the offshore jets (Areas 3 and 6). Because the offshore- and onshore-ward jets carried the biota from their origins, the biomass spectrum of zooplankton in an offshore jet inherited the dome-shaped biomass spectrum of a coastal cohort, and the spectrum in an onshore jet inherited the linear spectrum of an offshore cohort. Thus, the dome shape of the biomass spectra in the offshore eddies seen in Areas 2 and 3 was the result of *Pseudocalanus* spp. and *Calanus marshallae* being transported there from coastal upwelling zones. These coastal zooplankton communities can be entrapped in eddies and advected further into offshelf regions for hundreds of kilometers off the shelf and for hundreds of days (Huntley et al. 1995, 2000).

The offshore transport of coastal communities is indicated by the association between extending tongues of high zooplankton biomass from Heceta Bank and Cape Blanco, and the offshore currents (Figs. 5 & 6). In contrast, the onshore-ward currents transported low zooplankton-biomass waters to nearshore regions with zooplankton minima, such as the low zooplankton-biomass band south of Heceta Bank, extending from the offshore region to the coast (Fig. 6a) and corresponding to a negative gradient advection (Fig. 9). In the Heceta Bank region, these onshore and offshore transports led to a biomass convergence.

Coastal convergence and offshore export of zooplankton biomass

The transport flux estimates crossing the boundaries surrounding the coastal region were extremely sensitive to the current fields, especially the estimates at the 153 m isobath (Table 1). The current field from Barnes interpolation indicates significant

cross-isobath transport, while the current field from BDF interpolation is mostly parallel to the 153 m isobath, minimizing the cross-isobath transport. Based on these estimates, the major transport flux into the Oregon coastal region occurred at the northern boundary (Transect 1), where the California Current transports zooplankton biomass southward at rates of ~2.5×10^3 (Barnes interpolation) and 1.0×10^3 t C d^{-1} (BDF interpolations). Across the southern boundary (Transect 12), the transport flux was relatively small and negligible compared to the northern boundary. The offshore transport across the 153 m isobath was on the same order of magnitude as that across the northern boundary. The offshelf transport across the 153 m isobath computed from the currents based on Barnes interpolation was ~3.7×10^3 t C d^{-1}, 4 to 5 times higher than that based on BDF interpolation (~0.8×10^3 t C d^{-1}). Transport estimates were primarily different at the shelf break south of Heceta Bank. The smaller cross-isobaths transport from the current field based on BDF interpolation was caused by both the mesoscale currents being more parallel to the 153 m isobath and by the mesoscale returning currents associated with offshore jets. The cross-isobath transport of biota due to cross-isobath currents from Barnes interpolation occurred south of Heceta Bank and Cape Blanco.

The total zooplankton biomass integrated within the coastal area shallower than 153 m was ~4×10^4 t C. The net transport crossing the boundaries of this coastal area was -1.4×10^3 and 0.3×10^3 t C d^{-1} (using the current fields derived from Barnes and BDF interpolations, respectively), which equates to biomass accumulation rates of −0.04 and 0.01 d^{-1}, respectively. The different transport fluxes estimated using the 2 interpolation methods do not imply any unreliability of these mathematical methods, but instead indicate the differences between these methods in dealing with uncertainties in field data. Thus, to verify results from mathematical methods with field observations is necessary — despite being challenging — in order to study coupled physical and biological processes.

Comparing advection and growth, the growth rate of zooplankton is ~0.1 d^{-1} in 8°C water within upwelling areas using a general formula (Huntley & Lopez 1992, Hirst & Bunker 2003, Zhou et al. 2010, Bi et al. 2011), or 0.08 d^{-1} for copepod species from a time series in upwelling waters off Newport, Oregon (Gómez-Gutiérrez & Peterson 1999). The local specific convergence rates of biomass advection were between −0.5 and 0.5 d^{-1}, which were much higher than local zooplankton growth rates (Fig. 9b). The dominance of physical advective processes in zooplankton biomass variations indicates the difficulty of studying processes of zooplankton population dynamics *in situ*, since this requires following a specific zooplankton cohort. Although the local convergence rate is 5 times higher than the local growth rate, the area mean of convergence rates decreases when the convergence rate is integrated over a larger region. The accumulation rates due to the convergence of biomass gradient advection in the entire coastal area (shallower than 153 m) off Oregon were approximately −0.04 and 0.01 d^{-1} based on Barnes and BDF interpolations, respectively. These accumulation rates are ~1 order of magnitude smaller than the growth rate, indicating that the high zooplankton production in the Oregon coastal region was enhanced by local primary production.

The local convergence of zooplankton transport was dominated by advection of zooplankton gradients, because the convergence of currents was small and secondary. In the survey area, the advection of zooplankton biomass gradients showed alternating negative and positive patches associated with currents and biomass gradients (Fig. 9). The signs simply indicate the advection of a high biomass center or a low biomass center into a local area: In the offshore-ward jets, the positive sign indicates an offshore transport of nearshore-produced zooplankton biota, while in an onshore current, the negative sign indicates an intrusion of offshelf low zooplankton water. Thus, the mosaic of zooplankton gradient advection in Fig. 9 also represents the horizontal exchange-mixing processes of zooplankton nearshore and offshelf due to advective transports. These results, especially the different estimates using Barnes and BDF interpolations, show the nonlinearity of zooplankton gradient advection processes and the potential biases when using linear averaging to remove mesoscale features. Measurements of currents and biomass (and thus estimates of advection and population process rates) can only be improved to a certain extent. For example, vessel-based measurements are by the cruise speed and the maximum number of sensors that can be deployed at the same time. The recent development of autonomous underwater vehicles and miniaturized optical and acoustic sensors may allow higher spatial and temporal resolution of physical and biological fields. Most importantly, errors inherent in the sampling method and design must be analyzed prior to a cruise, so that they can be estimated and maybe even avoided.

CONCLUSIONS

The high-resolution observations of physical-biological fields in the California Current system off Oregon during June 2002 revealed strong relationships between coastal upwelling areas and zooplankton biomass maxima. Primary productivity in the coastal region was enhanced by upwelling, supporting the ecosystem in the region. However, the zooplankton productivity within the region not only depended on local growth and regeneration but also on the convergence of zooplankton biomass gradient advection. In the coastal area shallower than 153 m between 41° 44′ N and 44° 37′ N, the zooplankton biomass was ~4 × 10^4 t C. There were significant differences in transport flux estimates from different current fields based on Barnes and BDF interpolation methods, indicating inherent uncertainties in the field data and the importance of resolving these differences. Despite these discrepancies, the results indicate that the influx of zooplankton biomass into the coastal area occurred primarily at the northern boundary off Newport and was carried by the southward California Current. This biomass flux occurred at a rate of ~1 × 10^3 to 2.5 × 10^3 t C d^{-1} (specific rate of 0.03 to 0.06 d^{-1}) based on the 2 different analytical methods, which is close to the mean growth rate of zooplankton in upwelling areas (Huntley & Lopez 1992, Hirst & Bunker 2003, Zhou et al. 2010, Bi et al. 2011). The flux at the southern boundary was 1 order of magnitude less than that at the northern boundary. Offshore transport of high zooplankton biomass water was detected off Heceta Bank and Cape Blanco, while onshore intrusions of low zooplankton-biomass waters occurred between Heceta Bank and Coos Bay. The net offshore transport of zooplankton crossing the 153 m isobath was ~0.8 × 10^3 to 3.7 × 10^3 t C d^{-1} (specific rate of 0.02 to 0.09 d^{-1}), significantly contributing to the loss of coastal zoooplankton communities during early June 2002. Thus, along the Oregon coast, physical advection processes are on the same order of magnitude as the zooplankton growth rate and important in determining zooplankton retention and productivity.

Acknowledgements. We thank the Oregon State University marine tech group and crew of the R/V 'Thomas Thompson' for providing technical support in instrument integration. M.Z. and D.W. are also grateful for the zooplankton data provided by Dr. W. Peterson and his group. This research was supported by the United States National Science Foundation grant numbers OCE0002257 and OCE 0435581 to M.Z. and OCE0435619 to T.C.

LITERATURE CITED

Barnes SL (1964) A technique for maximizing details in numerical map analysis. J Appl Meteorol 3:396–409

Barth JA, Pierce SD, Smith RL (2000) A separating coastal upwelling jet at Cape Blanco, Oregon and its connection to the California Current System. Deep-Sea Res II 47: 783–810

Barth JA, Cowles TJ, Korso PM, Shearman RK, Huyer A, Smith RL (2002) Injection of carbon from the shelf to offshore beneath the euphotic zone in the California Current. J Geophys Res 107, doi:10.1029/2001JC000956

Barth JA, Pierce SD, Cowles TJ (2005) Mesoscale structure and its seasonal evolution in the northern California Current System. Deep-Sea Res II 52:5–28

Benfield MC, Lavery AC, Wiebe PH, Greene CH, Stanton TK, Copley NJ (2003) Distributions of physonect siphonulae in the Gulf of Maine and their potential as important sources of acoustic scattering. Can J Fish Aquat Sci 60:759–772

Benoit-Bird KJ, Au WW (2003) Echo strength and density structure of Hawaiian mesopelagic boundary community patches. J Acoust Soc Am 114:1888–1897

Beyer WH (ed) (1987) Handbook of mathematical sciences. CRC Press, Boca Raton, FL

Bi H, Feinberg L, Shaw CT, Peterson WT (2011) Estimated development times for stage-structured marine organisms are biased if based only on survivors. J Plankton Res 33:751–762

Bretherton FP, Davis RE, Fandry CB (1976) A technique for objective analysis and design of oceanographic experiments applied to MODE-73. Deep-Sea Res Oceanogr Abstr 23:559–582

Brink KH, Cowles TJ (1991) The coastal transition zone program. J Geophys Res 96:14637–14647

Dorland RD, Zhou M (2008) Circulation and heat fluxes during the austral fall in George VI Sound, Antarctic Peninsula. Deep-Sea Res II 55:294–308

Erofeeva SY, Egbert GD, Kosro PM (2003) Tidal currents on the central Oregon shelf: models, data, and assimilation. J Geophys Res 108:3148, doi:10.1029/2002JC001615

Fossheim M, Zhou M, Tande KS, Pedersen OP, Zhu Y, Edvardsen A (2005) Interactions between biological and environmental structures on the coast of northern Norway. Mar Ecol Prog Ser 300:147–158

Gómez-Gutiérrez J, Peterson WT (1999) Egg production rates of eight calanoid copepod species during summer 1997 off Newport, Oregon, USA. J Plankton Res 21: 637–657

Haidvogel DB, Beckmann A, Hedström KS (1991) Dynamical simulations of filament formation and evolution in the Coastal Transition Zone. J Geophys Res 96:15017–15040

Hawkins HF, Rosenthal SL (1965) On the computation of stream functions from the wind field. Mon Weather Rev 93:245–252

Herman AW (1992) Design and calibration of a new optical plankton counter capable of sizing small zooplankton. Deep-Sea Res 39:395–415

Hirst AG, Bunker AJ (2003) Growth of marine planktonic copepods: global rates and patterns in relation to chlorophyll a, temperature, and body weight. Limnol Oceanogr 48:1988–2010

Huntley ME, Lopez MDG (1992) Temperature-dependent production of marine copepods: a global synthesis. Am Nat 140:201–242

Huntley ME, Zhou M, Norhausen W (1995) Mesoscale distribution of zooplankton in the California Current in late spring observed by an Optical Plankton Counter. J Mar Res 53:647–674

Huntley ME, González A, Zhu Y, Zhou M, Irigoien X (2000) Zooplankton dynamics in a mesoscale eddy-jet system off California. Mar Ecol Prog Ser 201:165–178

Huyer A (1983) Coastal upwelling in the California current system. Progr Oceanogr 12: 259–284

Kosro PM, Huyer A (1986) CTD and velocity surveys of seaward jets off northern California, July 1981 and 1982. J Geophys Res 91:7680–7690

Kosro PM, Huyer A, Ramp SR, Smith RL and others (1991) The structure of transition zone between coastal waters and the open ocean off northern California, winter and spring 1987. J Geophys Res 96:14707–14730

Kundu PK, Allen JS (1976) Some three-dimensional characteristics of low-frequency current fluctuations near the Oregon coast. J Phys Oceanogr 6:181–199

Largier JL, Magnell BA, Winant CD (1993) Subtidal circulation over the northern California shelf. J Geophys Res 98: 18147–18179

Legendre L, Legendre P (eds) (1983) Numerical ecology. Dev Environ Model 20

Mackas DL, Washburn L, Smith SL (1991) Zooplankton community pattern associated with a California Current cold filament. J Geophys Res 96:14781–14797

McCreary JP, Fukamachi Y, Kundu PK (1991) A numerical investigation of jets and eddies near an eastern ocean boundary. J Geophys Res 96:2515–2534

Peterson WT, Gómez-Gutiérrez J, Morgan CA (2002) Cross-shelf variation in calanoid copepod production during summer 1996 off the Oregon coast, USA. Mar Biol 141: 353–365

Pickett MH, Paduan JD (2003) Ekman transport and pumping in the California Current based on the U.S. Navy's high-resolution atmospheric model (COAMPS). J Geophys Res 108:3327, doi:10.1029/2003JC001902

Pierce SD, Allen JS, Walstad LJ (1991) Dynamics of the Coastal Transition Zone Jet: 1. Linear stability analysis. J Geophys Res 96:14979–14994

Pierce SD, Smith RL, Kosro PM, Barth JA, Wilson CD (2000) Continuity of the poleward undercurrent along the eastern boundary of the mid-latitude north Pacific. Deep-Sea Res II 47:811–829

Platt T, Denman K (1978) The structure of pelagic marine ecosystems. Rapp P-V Réun Cons Int Explor Mer 173: 60–65

Rienecker MM, Mooers CNK (1989) Mesoscale eddies, jets, and fronts off Point Arena, California, July 1986. J Geophys Res 94:12555–12569

Rodriguez J, Mullin MM (1986) Relation between biomass and body weight of plankton in a steady state oceanic ecosystem. Limnol Oceanogr 31:361–370

Rudnick DL (1996) Intensive surveys of the Azores Front: 2. Inferring the geostrophic and vertical velocity fields. J Geophys Res 101:16291–16303

Shearman RK, Barth JA, Allen JS, Haney RL (2000) Diagnosis of the three-dimensional circulation in mesoscale features with large Rossby number. J Phys Oceanogr 30: 2687–2709

Sheldon RW, Parsons TR (1967) A continuous size spectrum for particulate matter in the sea. J Fish Res Board Can 24: 909–915

Sheldon RW, Prakash A, Sutcliffe WH Jr (1972) The size distribution of particles in the ocean. Limnol Oceanogr 17: 327–340

Sprules WG, Munawar M (1986) Plankton size spectra in relation to ecosystem productivity, size, and perturbation. Can J Fish Aquat Sci 43:1789–1794

Strub PT, Kosro PM, Huyer A (1991) The nature of the cold filaments in the California Current system. J Geophys Res 96:14743–14768

Ullman DS, Dale AC, Hebert D, Barth JA (2003) The front on the northern flank of Georges Bank in spring: 2. Cross-frontal fluxes and mixing. J Geophys Res 108:8010, doi: 10.1029/2002JC001328

van Geen A, Takesue RK, Gooddard J, Takahashi T, Barth JA, Smith RL (2000) Carbon and nutrient dynamics during coastal upwelling off Cape Blanco, Oregon. Deep-Sea Res II 47:975–1002

Washburn L, Kadko DC, Jones BH, Hayward T and others (1991) Water mass subduction and the transport of phytoplankton in a coastal upwelling region. J Geophys Res 96:14927–14945

Wiebe PH, Beardsley RC, Bucklin A, Mountain DG (2001) Coupled biological and physical studies of plankton populations in the Georges Bank region and related North Atlantic GLOBEC study sites. Deep-Sea Res II 48:1–2

Zhou M (1998) An objective interpolation method for spatiotemporal distribution of marine plankton. Mar Ecol Prog Ser 174:197–206

Zhou M, Huntley ME (1997) Population dynamics theory of plankton based on biomass spectra. Mar Ecol Prog Ser 159:61–73

Zhou M, Zhu Y, Putnam S, Peterson J (2001) Mesoscale variability of physical and biological fields in southeastern Lake Superior. Limnol Oceanogr 46:679–688

Zhou M, Zhu Y, Tande KS (2005) Circulation and behavior of euphausiids in two Norwegian sub-Arctic fjords. Mar Ecol Prog Ser 300:159–178

Zhou M, Tande KS, Zhu Y, Basedow S (2009) Productivity, trophic levels and size spectra of zooplankton in northern Norwegian shelf regions. Deep-Sea Res II 56:1934–1944

Zhou M, Carlotti F, Zhu Y (2010) A size-spectrum zooplankton closure model for ecosystem modelling. J Plankton Res 32:1147–1165

Zhu Y, Tande KS, Zhou M (2009) Mesoscale physical processes and zooplankton productivity in the northern Norwegian shelf region. Deep-Sea Res II 56:1922–1933

Editorial responsibility: Kenneth Sherman, Narragansett, Rhode Island, USA

Submitted: November 11, 2013; Accepted: April 24, 2014
Proofs received from author(s): July 12, 2014